Journal of Materials Chemistry A

Accepted Manuscript

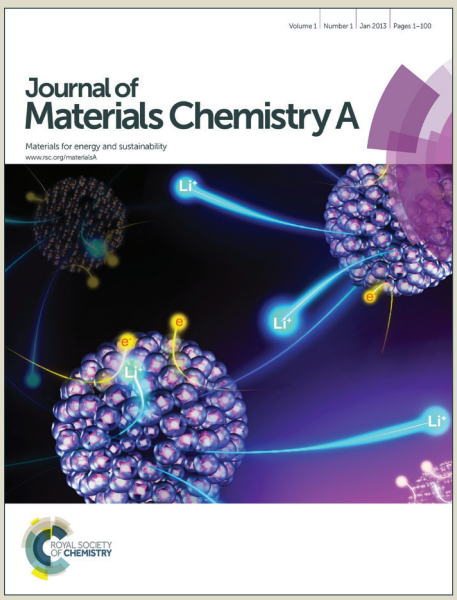

ROYAL SOCIETY OF CHEMISTRY

www.rsc.org/materialsA

Journal of Materials Chemistry A RSCPublishing

ARTICLE

Flexible CoO-graphene-carbon nanofiber mats as binder-free anodes for lithium-ion batteries with superior rate capacity and cyclic stability

Ming Zhang,[*ab] Feilong Yan,[a] Xuan Tang,[a] Qiuhong Li,[a] Taihong Wang[*a] and Guozhong Cao[*b]

Cite this: DOI: 10.1039/xoxxoooooox

Received ooth January 2014,
Accepted ooth January 2014

DOI: 10.1039/xoxxoooooox

www.rsc.org/

The flexible mats composed of CoO-graphene-carbon nanofibers are prepared by electrospinning and subsequent thermal treatment. The flexible mats of CoO-graphene-carbon annealed at 650 °C show discharge capacities of 760 and 690 mA h/g at 252nd and 352nd cycle at a current density of 500 mA/g, much higher than those of pure carbon nanofibers, graphene-carbon nanofibers, and CoO-carbon nanofibers at the respective cycles. The CoO-graphene-carbon can deliver a discharge capacity of 400 mA h/g at a current density of 2 A/g, also higher than those of CoO-carbon and graphene-carbon nanofibers. The improved electrochemical properties of CoO-graphene-carbon nanofiber flexible mats could be ascribed to the frameworks for the fast diffusion of Li^+, the graphene to enhance the conductance and the mechanical property of the mats, and the defective sites arising from the introduced CoO and graphene to storage Li^+. It is believed that the electrospinning method combined with graphene could be a useful approach to prepare flexible mats for lithium-ion batteries, supercapacitors, and fuel cells.

1 Introduction

Flexible devices are of great advantages because of potential low-cost production, and have been investigated by various groups.[1, 2] It is of great signification to develop flexible energy-storage equipment to meet the energy demand of flexible devices.[3, 4] Lithium-ion batteries (LIBs) are promising candidates in this area because of their intrinsic high energy density, relative high power density, and environmentally friendly.[5-7] Accommodating frequent mechanical strains and retaining high quality energy supply for long-time use is a very important aspect of flexible electrodes for LIBs. Generally, the current LIBs electrodes are non-flexible, and still suffer from insufficient rate capacity, and inferior cyclic stability, especially most of anodes.[8-11] It is highly desirable to develop flexible electrodes with high properties for LIBs.

Carbon materials, especially the graphene and carbon nanofibers, have been demonstrated to be flexible electrodes for energy storage.[12, 13] Carbon nanofibers with much space among them have drawn more attention because they are of benefit for the fast diffusion of Li^+ compared with flexible graphene sheets.[8, 9, 14, 15] However, their specific capacities are too low to satisfy the energy demand of human because of their low theoretical capacity.[14] Modifying carbon materials with other materials of high theoretical capacity or introducing defective sites (or micropores) are effective ways to improve their properties.[16-22] Cobalt oxide with different morphology has been studied in the field of LIBs by many researchers recently owing to its relative high specific capacity.[23-25] Cobalt compound-carbon nanofibers composites also have been the research hot-pot of LIBs.[17, 19, 26, 27] Unfortunately, carbon nanofibers may become fragile after cobalt oxide being added in, resulting in the scissile anodes.[28]

Graphene, a new kind of 2-D carbon material, possesses excellent properties, such as excellent mechanical property, high conductivity, and good stability.[29] Many studies about graphene-based composites have been published regarding the energy storage.[30-34] For example, graphene could improve the mechanical property of the nanofibers made by electrospinning.[35, 36] Besides, graphene in electrospun nanofibers could be employed as a conductive additive to enhance the conductance of the nanofibers, resulting in improved properties.[32, 37] Nevertheless, preparing graphene-based nanofibers with excellent properties is not an easy task because the dispersion of graphene is poor in the solvent for electrospinning.

In this study, the flexible mats of CoO-graphene-carbon (CoO-G-C) nanofibers were synthesized by electrospinning and following careful thermal treatment. The precursor of graphene was processed by a special method to improve its dispersion in

organic solvent for electrospinning. Although the content of graphene and CoO in the nanofibers ware very low, the flexible mats as binder-free anodes for LIBs showed high specific capacity at a large current density, and excellent cyclic stability. The research results demonstrated that the effects of graphene on the properties of the mats included many aspects.

2 Experimental

2.1 Materials synthesis

Polyacrylonitrile (PAN, MW=150 000, Sigma-Aldrich Co., Ltd., USA), Cobalt (II) acetate tetrahydrate ($CoAc_2$, Alfa Aesar Co., Ltd., USA), and N, N-dimethylformamide (DMF, J. T. Baker Co., Ltd., USA) were used without any purification. Graphene oxide (GO) was prepared according to previous literature.[38, 39] To enhance the dispersion of GO in DMF, the GO suspension was centrifuged and cleared by DMF for several times. Then GO was dispersed in DMF with a concentration of about 0.4 mg/ml. After that, the suspension was processed by ultrasonic wave for 30 min. To prepare the precursor solution for electrospinning, PAN, $CoAc_2$, and GO were dissolved in DMF to form the solution with the concentrations of 6.5 wt%, 2.5 wt% and 0.066 mg/mL. To prepare pure carbon fibers, the precursor without $CoAc_2$ and GO also was prepared. The precursor for nanofibers without graphene was prepared in the similar way except the GO. All the precursor solution was transferred into a 3 mL springe with a stainless steel needle (0.6 mm in the inner diameter). A syringe pump controlled the flow rate of the precursor solution to about 0.3 mL/h. An aluminum foil as the collector was vertically positioned at 15 cm away from the needle. The needle was connected to a high voltage DC power to get a voltage of 13-17 kV. Under these conditions, pure PAN, PAN-GO, PAN-$CoAc_2$, PAN-GO-$CoAc_2$ nanofibers were generated, and formed the mats. After being pre-oxidized at 225 ^oC in air for 6 h, the resulting brown films (PAN-GO-$CoAc_2$) were treated at 550-650 ^oC in nitrogen for 2 h to carbonize the PAN and/or decompose the $CoAc_2$, and the products were marked as CoO-G-C. The pure PAN, PAN-GO, and PAN-$CoAc_2$ nanofibers were treated in the similar way at 650 ^oC to obtain the samples. The final pure carbon, graphene-carbon, CoO-carbon (CoO-C) nanofibers were marked as E650, F650, and C650, respectively.

2.2 Materials characterization

The microstructure of the samples were characterized using a JEOL JSM-7000F scanning electron microscope (SEM), and a FEI Tecnai G2 F20 transmission electron microscope (TEM) operating at 200 kV accelerating voltage. The samples also were analyzed by X-ray photoelectron spectroscopy (XPS, Surface Science Instruments S-probe spectrometer). The binding energy scales were calibrated by assigning the lowest binding energy C1s peak (a binding energy of 285.0 eV). Elemental analysis of samples was achieved using energy dispersive spectroscopy (EDS).

2.3 Electrochemical measurements

The mats (including pure carbon, graphene-carbon, CoO-C, and CoO-G-C nanofibers) were directly used as binder-free anodes for electrochemical measurements towards the storage of Li^+. The Celgard 2400 microporous polypropylene membrane was used as a separator to assemble coin cells (CR 2016). The electrolyte consisted of a solution of 1 M $LiPF_6$ in ethylene carbonate/dimethyl carbonate (1:1, in volume). Pure lithium

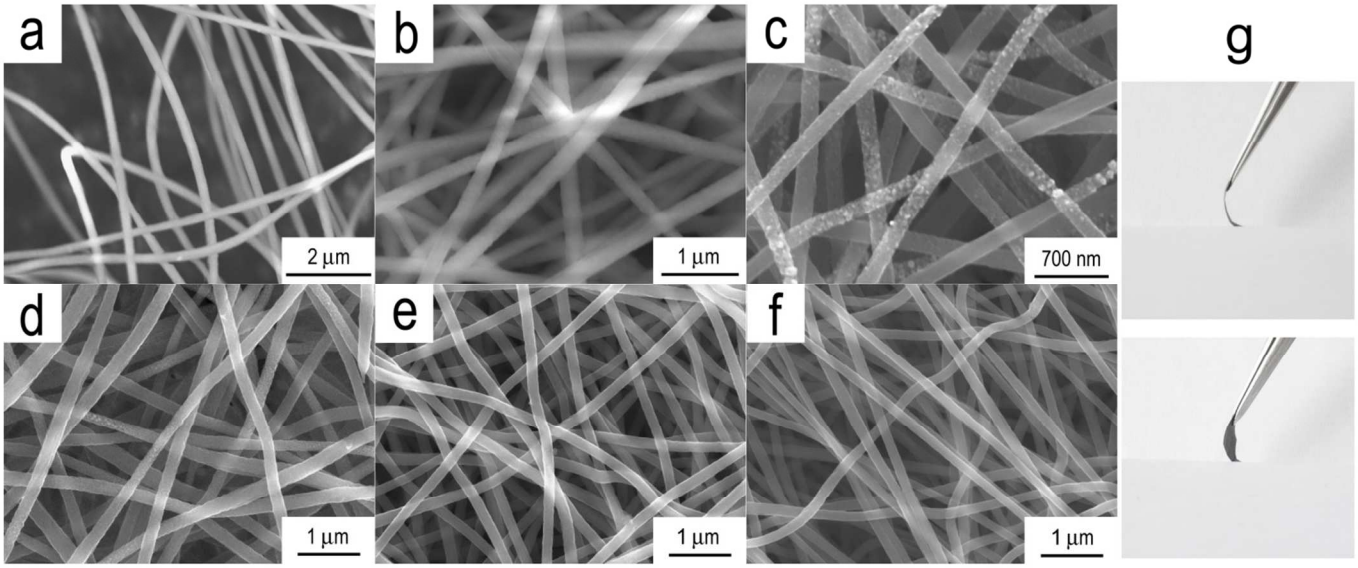

Fig. 1 SEM images of the as-prepared (a), treated at 225 ^oC (b), and annealed at 650 ^oC CoO-G-C nanofibers(c). SEM images of the nanofibers annealed at 650 ^oC: (d) CoO-C, (e) pure carbon, (f) graphene-carbon. The digital photos to show the flexibility of CoO-G-C mats are displayed in (g).

foils were used as both the counter and the reference electrodes. All the cells were assembled in an argon-filled glove-box with the moisture and the oxygen levels less than 1 ppm. The discharge and charge measurements were carried out using an Arbin BT2000 and a LAND battery testing system with the cut off potentials being 0.01 V for discharge and 3 V for charge. All the specific capacities in this study were calculated based on the weight of the mats. The cyclic voltammetry results were collected on the electrochemical workstation (CHI660B).

3 Results and discussion

3.1 Synthesis and Characterization of CoO-G-C mats

Fig. 1a shows the SEM image of the as-prepared PAN-GO-$CoAc_2$ nanofibers. The noodle-like nanofibers with a diameter of about 220 nm easily changed their position during the measurement, showing their less stability under the electron beam bombardment and poor conductance. After treated at 225 ^oC, the nanofibers without any obvious nanoparticles decrease to nearly 200 nm. Bright spots in the SEM images of Fig. 1a and 1b were due to the accumulated charges and suggested the relatively poor conductance of the nanofibers. The SEM image of the CoO-G-C nanofibers is shown in Fig. 1c. The nanofibers with diameters of approximate 165 nm are composed of disperaed nanoparticles and graphene in the carbon nanofiber matrix. Although the graphene is not directly observed in the SEM image, the GO could be reduced to graphene by thermal treatment.[40] The diameters of the CoO-G-C nanofibers decrease from 220 to 165 nm, which could be attributed to the decomposition of PAN and $CoAc_2$, as shown in Fig. S1. In a comparison experiment, no GO was added, and the final samples (CoO-C) were shown in Fig. 1d. The diameters of CoO-C nanofibers were approximate 175 nm. Besides, the nanoparticles on the CoO-C nanofibers are much less obvious than those on the CoO-G-C nanofibers. The pure carbon nanofibers (Fig. 1e) and graphene-carbon nanofibers (Fig. 1f) were similar to each other. The smaller diameters of graphene-carbon nanofibers could be ascribed to the polarity of GO. The digital photos of CoO-G-C mats are shown in Fig. 1g. The sectional view of the mats indicates that they are highly flexible. The photo from another angle displays that there are no cracks on the mats, showing the flexibility of the CoO-G-C further.

TEM was used to characterize the micromorphology of the samples. Fig. 2a shows a TEM image of CoO-G-C nanofibers. The nanofibers are about 165 nm, and the nanoparticles on the nanofibers are very small. Obviously, the distribution of nanoparticles is inhomogenous on the nanofibers compared with a previous report.[17] This phenomenon may be attributed to the oxygen-containing groups on GO that affected the nucleation and growth of CoO nanoparticles. An amplified image is shown in Fig. 2b. The surface of nanofibers is rough with enlarged surface area and porosity. Besides, the nanoparticles are homogenously distributed in this micro-area. This special phenomenon could be attributed to graphene (although no graphene was observed) because of the effects of graphene on the morphology of nanomaterials.[41] The high-resolution TEM image is shown in Fig. 2c. The nanoparticles are as small as about 5nm. The d-spacing of the planes is 0.246 nm, which is very close to that of (111) plane for CoO (JCPDS 48-1719), implying that the nanoparticles are CoO. No graphene sheets are observed by TEM. A possible reason is that graphene sheets with a low ratio in the composites are covered up by carbon arising from PAN. Similar results could be found in literature about graphene-carbon composites.[32, 42] The microstructure of the CoO-G-C nanofibers is proposed based on above result, schematically shown in Fig. 2d. The graphene could control the nucleation and growth of CoO nanoparticles. The inhomogeneous distribution of graphene on the nanofibers results in the nonuniform dispersion of very small CoO nanoparticles, which is different from the CoO-C fibers without graphene.[17]

XPS analysis was carried out on a Surface Science Instruments S-probe spectrometer to elucidate the bond state of CoO-G-C samples prepared at 650 ^oC (marked as A650). Before the measurement, this instrument has a monochroma-

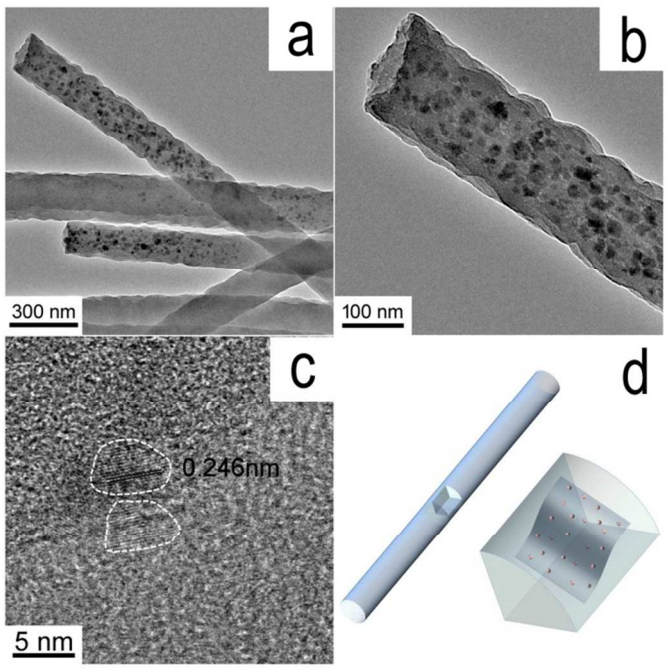

Fig. 2 a), b), and c) show TEM images of CoO-G-C (A650) nanofibers at different magnification. d) A schematic diagram showing the inhomogeneous distribution of CoO nanoparticles on CoO-G-C nanofibers.

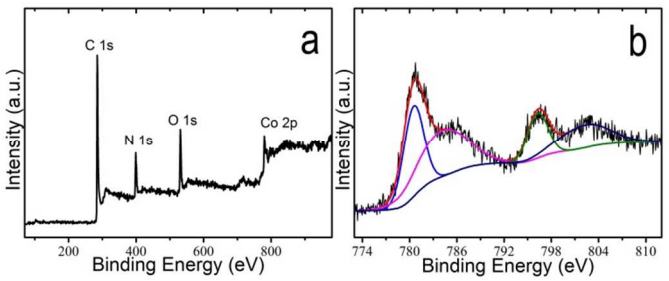

Fig. 3 (a) XPS spectra of CoO-G-C nanofiber mats (A650) obtained at 650 ^oC; (b) The fine XPS spectrum of Co 2p indicates that the cobalt are Co^{2+}.

tized Al K_α X-ray and a low energy electron flood gun for charge neutralization of non-conducting samples. The XPS spectra of A650 in Fig. 3a exhibit four main peaks at about 285.0, 398.6, 531.5 and 780.4 eV, corresponding to the peaks of C 1s, N 1s, O 1s and Co 2p.[43-46] These results are highly consistent with those of EDS (as shown in Fig. S2) that there are four elements in them. The fine XPS spectra of Co 2p in Fig. 3b exhibit two peaks at 780.4 and 796.2 eV associated with two satellite peaks, which are similar to previous reports about CoO.[43, 44] The $2p_{3/2}$ peak at about 780.4 eV can be indexed to Co^{2+} coordinated to oxygen anions.[44] The satellite peak arising from the occurrence of a ligand-to-metal charge transfer during the photoemission process was used as a fingerprint for the recognition of high-spin Co (II) species in A650.[46] The above peak patterns and relative intensities of Co 2p matched well with XPS spectra for well-identified CoO standards in literature, demonstrating that these particles were CoO further.[43, 44, 46] In Fig. S3a, the peaks at 531.5 and 533.4 eV indicated the presence of oxygen-containing groups on the surface.[45, 47] The O 1s peak at about 530 eV which corresponds to oxygen species in the spinel cobalt oxide phase (Co_3O_4) is not found, showing that the nanoparticles are CoO from another direction.[48] The fine XPS spectra of N 1s are shown in Fig. S3b. They are the residual group of PAN according to the raw materials. The N 1s peaks at 398.6 and 400.3 eV are assigned to pyridine-type and conjugated nitrogen.[49] Both of above nitrogen have positive effects on the storage of Li^+, especially the pyridine-type nitrogen.[50, 51] The fine XPS spectra of C 1s are shown in Fig. S3c. The C 1s spectra could be deconvoluted to five peaks, including the peaks at 285 (graphitized carbon), 286.5 (carbon in phenolic and alcohol groups), 288 (carbon in carbonyl or quinine groups), 289.2 (carbon in carboxyl or ester groups), and 290.4 eV (carbon in adsorbed CO and CO_2). Similar results have been reported by a previous study about PAN-based carbon nanofibers,[52] indicating that there are some oxygen-containing groups on the nanofibers.

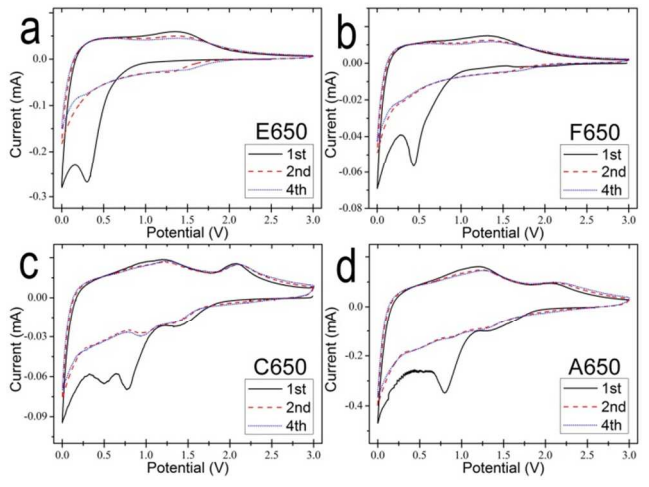

Fig. 4 CV curves of the samples CoO-G-C (A650), CoO-C (C650), pure carbon (E650), and graphene-carbon (F650) nanofibers at a scan rate of 0.3 mV/s.

3.2 Electrochemical Properties of CoO-G-C mats

CV measurements were carried out over a voltage range of 0-3 V to investigate the electrochemical mechanism, and the results are shown in Fig. 4. In Fig. 4a, the cathodic peak in the first cycle of E650 at about 0.4 V could be attributed to the formation of irreversible solid electrolyte interface (SEI) films. There are two anodic peaks at about 0.2 (not obvious in the first cycle) and 1.3 V, which could be indexed to the lithium extraction from graphite-like carbon and the delithiation of the defective sites on the carbon nanofibers, respectively.[21, 22, 53] The CV curve of the second cycle nearly overlapped with the curve in the fourth cycle, showing the good cyclic stability of E650. The CV curves of F650 in Fig. 4b are similar to those of E650, shown that graphene has little effect on the electrochemical reaction of carbon. The CV curves of C650 and A650 nanofibers are shown in Fig. 4c and 4d. During the first cycle, the cathodic peaks at about 1.35 V could be attributed to electrochemical reduction reaction of CoO with Li.[11, 20] The peaks in the range of 0.5-0.9 V could be ascribed to the formation of SEI films.[20] The CV curves of both A650 and C650 show three anodic peaks at about 0.2, 1.25, and 2.1 V, which could be indexed to the delithiation of carbon, the extraction of Li from the defective sites, and the reformation of CoO.[9, 20, 54] The difference in the CVs between A650 and C650 is that the delithiation peak of CoO in C650 is more obvious than that of A650, which may be attributed to the smaller particle size of CoO in C650 (Fig. S4). The anodic peaks (at about 1.25 V) of carbon in A650 and C650 shift to a low potential compared with pure carbon (E650), which could be attributed to the active effects of CoO on the carbon.[18] Besides, the anodic peaks for the delithiation of the defective sites at about 1.25 V of both A650 and C650 are stronger and broader than those of E650 and F650, indicating that more defective sites are introduced in the nanofibers with the presence of CoO.[53] The nearly overlapped CV curves of A650 and C650 in the 2^{nd} and 4^{th} cycles show good cyclic stability during the following cycles, demonstrating that graphene-carbon nanofibers are desirable frameworks for the anodes of LIBs. The difference between A650 and C650 is that the cathodic peak for the lithiation/delithiation of CoO in A650 shift to a low potential and its anodic peak shifts to a high potential compared to those peaks for the CoO in C650, showing a larger size of CoO in A650 which is consistent with the results of TEM (as shown in Fig. S4).[55] A previous study has demonstrated that graphene oxide could affect the morphology and size of the nanoparticles.[41] Therefore, the larger CoO nanoparticles size in A650 may be ascribed to the presence of graphene oxide in the precursor.

Fig. 5a compares the discharge capacities of samples (A650, C650, E650, and F650) as a function of cyclic number at different current densities. All of them show relative good cyclic stability during the cycles. Whereas, their discharge capacities at a current density of 0.1 A/g decrease from 1030 mA h/g (A650) to 520 mA h/g (E650). When the current

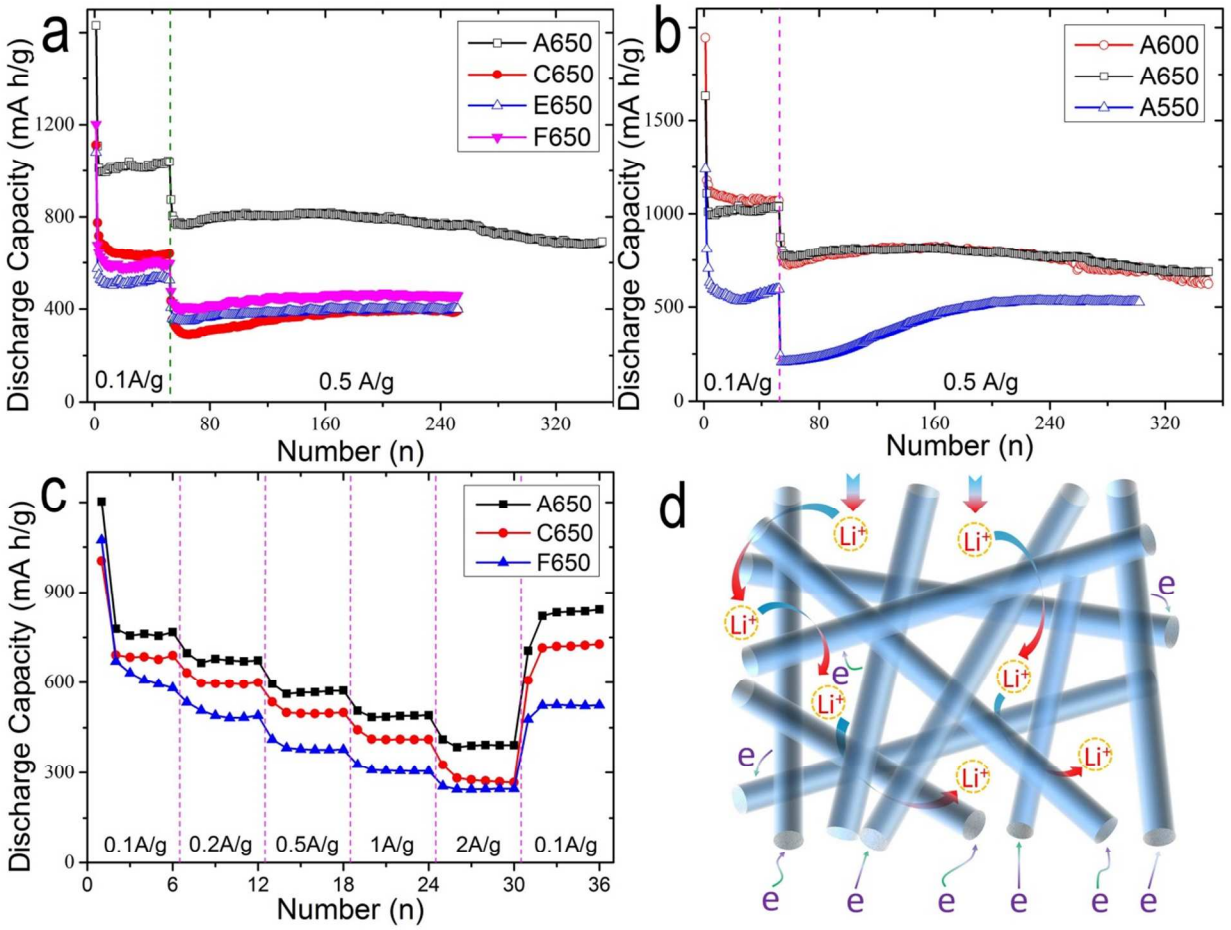

Fig. 5 (a) The cyclic properties of samples A650 (CoO-G-C), C650 (CoO-C), E650 (pure carbon), and F650 (graphene-carbon). (b) The discharge capacity vs. cyclic number curves of the samples A650, A600, and A550. (c) The rate capacity of the samples A650, C650, and F650. (d) A schematic diagram to show that the A650 nanofiber flexible mats are of benefit for the storage of Li^+.

density increases to 0.5 A/g, the corresponding discharge capacities go down from 760 mA h/g (A650) to 395 mA h/g (C650) at the 252nd cycle. In additional, the A650 could deliver a discharge capacity of 690 mA h/g at the 352nd cycle, showing super cyclic stability and high capacity. According to the TGA results (Fig. S5), the mass ratio of CoO in the both C650 and A650 are about 29.5%, showing the less effects of graphene on the mass ratio of CoO in the nanofibers. A more interesting phenomenon is that the discharge capacity of A650 is much higher than those of both C650 and F650, demonstrating that the synergies among the three compositions (carbon, graphene, and CoO) is the critical factor in improving the electrochemical properties of the nanofiber mats. The discharge capacity of A650 also is higher than the theoretical specific capacity of CoO-G-C calculated to be 533 mA h/g based on the 29.5 wt% of CoO and 70.5 wt% carbon (457 mA h/g, according to F650 after 252 cycles), which is another evidence of the synergies effects in the CoO-G-C. Comparing C650 with F650, it is clear that the discharge capacity of C650 is higher than that of F650 at a current of 0.1 A/g, and it was inverted. This phenomenon demonstrates that CoO play as a key factor in the improvement of capacity while the graphene have more influence on the enhancement of rate capacities. Based on the results from CV curves, the superior of A650 could be ascribed to the improved defective sits in A650. Comparing the properties of A650 with previous reports about CoO_x-C fibers arising from PAN,[17, 19, 26, 27] it could be found that the CoO-G-C mats (A650) showed a relatively high specific capacity and superior cyclic stability, as shown in **Table 1**. Besides, their properties also are better than some of CoO_x-graphene and CoO_x-C composites towards the storage of Li^+ (as shown Table S1),[25, 45, 56-62] indicating the advantages of CoO-G-C mats as binder-free anodes for LIBs further.

The effects of the annealed temperature on the properties of CoO-G-C also were investigated, and the results are shown in Fig. 5b. Although the high temperature (>700 °C) will result in the carbon fibers with high conductance,[8] the CoO-G-C nanofibers are obtained at 550, 600, and 650 °C to avoid the conversion of CoO to Co and the reduce of nitrogen, and the samples are marked as A550, A600, and A650, respectively. It can be found from the Fig. 5b that the capacities of A600 and A650 are much higher than that of A550, especially at a small

Table 1. The specific capacities and cyclic properties of CoO_x-carbon composites as anodes for LIBs.

Materials	Capacity (mA h/g)/Current density (A/g)			Ref.
	50th	100th	Others	
Co-C fibers[(a)]	804 / 0.1			[24]
Co_3O_4-C fibers[(a)]	534 / 0.1 20th			[26]
CoO-C fibers[(a)]	633 / 0.1 52nd			[27]
CoO-C fibers[(a)]		853 / 0.14		[17]
Co_3O_4-CNT		530 / 0.09		[25]
CoO-Graphene			640 / 0.1 150th	[56]
CoO-C		725 / 0.2		[57]
CoO-C	700 / 0.1 70th			[58]
Co_3O_4-Graphene		732 / 0.15		[59]
CoO-Graphene	1592 / 0.05			[60]
CoO-Graphene	935 / 0.05			[45]
Co_3O_4-Graphene		1005 / 0.074		[61]
Co_3O_4-CMK3	709 / 0.1 20th			[62]
CoO-G-C mats[(a)]		800 / 0.5	690 / 0.5 352nd	This study

[(a)] PAN-based fibers

current density. The inferior property of A550 could be attributed the low carbonization degree and poor conductance of the nanofibers. The properties of A650 are just a little better than those of A600, showing that the best annealed temperature for CoO-G-C is in the range of 600 to 650 °C. This result consists with a recent study about PAN-based carbon for LIBs.[51] According to the SEM images (Fig. S6), the porosity of CoO-G-C improves from A550 to A650. Therefore, to achieve a best electrochemical property of CoO-G-C, an optimal temperature is to balance the porosity and the conductance of the nanofibers. To study the advance of the CoO-G-C flexible mats as anodes for LIBs, the rate capacities were evaluated, as shown in Fig. 5c. The CoO-G-C (A650) keeps reversible capacities of 770, 680, 570, 490, and 400 mA h/g at current densities of 0.1, 0.2, 0.5, 1, and 2 A/g, respectively. These values are higher than those of CoO-C (C650) at the corresponding current densities. The improvement could be attributed to the enhanced conductance arising from graphene. The property of CoO-G-C is also better than that of pure carbon (E650), showing the positive effects of CoO nanoparticles on the electrochemical property of the nanofibers.

Above results have demonstrated that CoO-G-C flexible mats showed improved properties towards the storage of Li^+. The improvement could be attributed to following reasons based on their microstructure, as shown in Fig. 5d. Firstly, the CoO-G-C nanofiber mats with large pores are facile for the diffusion of Li^+.[63] Secondly, the mats of carbon fibers are of high conductance for the transfer of electrons, and decrease the polarization at a large current density. Thirdly, the graphene of good conductive could improve the conductance of the nanofibers.[37] Fourthly, the graphene can control the particle size of CoO and maintain the structural stability of CoO nanoparticles.[31] Fifthly, the graphene with superior mechanical properties could enhance the mechanical strength of the nanofibers and protect them from the fracture.[36] Sixthly, the flexible mats can accommodate a large deformation without rupture. Seventhly, the flexible mats as binder-free anodes for LIBs could reduce the internal resistance of the battery and provide a high output voltage. Eighthly, the CoO and graphene could introduce the defective sites in carbon nanofiber mats, resulting in the improvement of capacities for Li^+ storage.

4 Conclusions

Flexible mats of CoO-G-C nanofibers are synthesized by electrospinning and following thermal treatment. The results demonstrated that graphene could control the particle size of CoO during the synthesis procedure. As binder-free anodes for LIBs, the flexible mats of CoO-G-C nanofibers showed improved cyclic stability along with a high specific capacity (690 mA h/g after 352 cycles at a current density of 500 mA/g) and enhanced rate capacity (400 mA h/g at a current density of 2 A/g) compared with CoO-C, graphene-carbon, and pure carbon nanofibers mats. The improvement could be attributed to the mats for the fast diffusion of Li^+, the graphene which of good mechanical properties and superior conductance could not only control the particle size of CoO, but also improve the mechanical strength and conductivity of the flexible mats, and the defective sites arising from the introduced CoO and graphene to storage Li^+.

Acknowledgements

This research work has been financially supported in part by the National Science Foundation (NSF, CMMI-1030048), NESAC/BIO (EB-002027), and the University of Washington TGIF grant. Part of this work was conducted at the University of Washington NanoTech User Facility, a member of the NSF National Nanotechnology Infrastructure Network (NNIN). Ming Zhang would like to acknowledge the National Natural Science Foundation of China (61376073 and 21103046), the Hunan Provincial Natural Science Foundation of China (10JJ1011 and 11JJ7004), the China Scholarship Council and Fundamental Research Funds for the Central Universities.

Notes and references

[a] Key Laboratory for Micro-Nano Optoelectronic Devices of Ministry of Education and State Key Laboratory for Chemo/Biosensing and

Chemometrics, Hunan University, Changsha, 410082, P.R. China. Email: zhangming@hnu.edu.cn; thwang@hnu.edu.cn

[b] Department of Materials Science & Engineering, University of Washington, Seattle, Washington, 98195, USA. Email: gzcao@uw.edu

Electronic Supplementary Information (ESI) available: [the diameter distribution of nanofibers, EDS spectra of the CoO-G-C nanofiber mats (A650), the fine XPS spectra of O 1s, N 1s, and C 1s in CoO-G-C nanofibers (A650), TEM images of the CoO-G-C (A650) and CoO-C (C650), the TG curves of the CoO-G-C (A650) and CoO-C (C650) nanofiber, the SEM images of the CoO-G-C samples annealed at different temperatures, the table to summarize the specific capacity and cyclic properties of CoO_x-carbon composites]. See DOI: 10.1039/b000000x/

1. X. Li, T. Gu and B. Wei, *Nano Lett.*, 2012, **12**, 6366-6371.
2. X. Jia, Z. Chen, A. Suwarnasarn, L. Rice, X. Wang, H. Sohn, Q. Zhang, B. M. Wu, F. Wei and Y. Lu, *Energy Environ. Sci.*, 2012, **5**, 6845-6849.
3. D. Kuang, J. r. m. Brillet, P. Chen, M. Takata, S. Uchida, H. Miura, K. Sumioka, S. M. Zakeeruddin and M. Gra□tzel, *ACS Nano*, 2008, **2**, 1113-1116.
4. F. Zhang, C. Yuan, J. Zhu, J. Wang, X. Zhang and X. W. Lou, *Adv. Funct. Mater.*, 2013, **23**, 3909-3915.
5. Y. Liu, M. Clark, Q. Zhang, D. Yu, D. Liu, J. Liu and G. Cao, *Adv. Energy Mater.*, 2011, **1**, 194-202.
6. J. Song, S. Chen, M. Zhou, T. Xu, D. Lv, M. L. Gordin, T. Long, M. Melnyk and D. Wang, *J. Mater. Chem. A*, 2014, **2**, 1257-1262.
7. D. Yu, C. Chen, S. Xie, Y. Liu, K. Park, X. Zhou, Q. Zhang, J. Li and G. Cao, *Energy Environ. Sci.*, 2011, **4**, 858-861.
8. J. K. Lee, K. W. An, J. B. Ju, B. W. Cho, W. I. Cho, D. Park and K. S. Yun, *Carbon*, 2001, **39**, 1299-1305.
9. L. W. Ji and X. W. Zhang, *Nanotechnology*, 2009, **20**, 155705.
10. W. Y. Li, L. N. Xu and J. Chen, *Adv. Funct. Mater.*, 2005, **15**, 851-857.
11. J. Jiang, J. Liu, R. Ding, X. Ji, Y. Hu, X. Li, A. Hu, F. Wu, Z. Zhu and X. Huang, *J. Phys. Chem. C*, 2009, **114**, 929-932.
12. V. Presser, L. Zhang, J. J. Niu, J. McDonough, C. Perez, H. Fong and Y. Gogotsi, *Adv. Energy Mater.*, 2011, **1**, 423-430.
13. S. Chen, J. Duan, Y. Tang and S. Zhang Qiao, *Chem. Eur. J.*, 2013, **19**, 7118-7124.
14. C. Kim, K. S. Yang, M. Kojima, K. Yoshida, Y. J. Kim, Y. A. Kim and M. Endo, *Adv. Funct. Mater.*, 2006, **16**, 2393-2397.
15. B. Zhang, Y. Yu, Z. Huang, Y.-B. He, D. Jang, W.-S. Yoon, Y.-W. Mai, F. Kang and J.-K. Kim, *Energy Environ. Sci.*, 2012, **5**, 9895-9902.
16. M. Zhang, D. Lei, X. Yin, L. Chen, Q. Li, Y. Wang and T. Wang, *J. Mater. Chem.*, 2010, **20**, 5538-5543.
17. W.-H. Ryu, J. Shin, J.-W. Jung and I.-D. Kim, *J. Mater. Chem. A*, 2013, **1**, 3239-3243.
18. J. Yue, X. Zhao and D. Xia, *Electrochem. Commun.*, 2012, **18**, 44-47.
19. L. Wang, Y. Yu, P.-C. Chen and C.-H. Chen, *Scripta Materialia*, 2008, **58**, 405-408.
20. F. Li, Q.-Q. Zou and Y.-Y. Xia, *J. Power Sources*, 2008, **177**, 546-552.
21. N. Takami, A. Satoh, M. Oguchi, H. Sasaki and T. Ohsaki, *J. Power Sources*, 1997, **68**, 283-286.
22. Y.-P. Wu, C.-R. Wan, C.-Y. Jiang, S.-B. Fang and Y.-Y. Jiang, *Carbon*, 1999, **37**, 1901-1908.
23. J.-S. Do and C.-H. Weng, *J. Power Sources*, 2005, **146**, 482-486.
24. Y. Ding, P. Zhang, Z. Long, Y. Jiang, J. Huang, W. Yan and G. Liu, *Mater. Lett.*, 2008, **62**, 3410-3412.
25. G. Wang, X. Shen, J. Yao, D. Wexler and J.-H. Ahn, *Electrochem. Commun.*, 2009, **11**, 546-549.
26. P. Zhang, Z. P. Guo, Y. Huang, D. Jia and H. K. Liu, *J. Power Sources*, 2011, **196**, 6987-6991.
27. M. Zhang, E. Uchaker, S. Hu, Q. Zhang, T. Wang, G. Cao and J. Li, *Nanoscale*, 2013, **5**, 12342-12349.
28. L. Wang, Y. Yu, P. C. Chen, D. W. Zhang and C. H. Chen, *J. Power Sources*, 2008, **183**, 717-723.
29. M. J. Allen, V. C. Tung and R. B. Kaner, *Chem. Rev.*, 2010, **110**, 132-145.
30. M. Zhang, B. Qu, D. Lei, Y. Chen, X. Yu, L. Chen, Q. Li, Y. Wang and T. Wang, *J. Mater. Chem.*, 2012, **22**, 3868-3874.
31. C. H. Kim, B.-H. Kim and K. S. Yang, *Carbon*, 2012, **50**, 2472-2481.
32. Z. Tai, X. Yan, J. Lang and Q. Xue, *J. Power Sources*, 2012, **199**, 373-378.
33. J. Liang, Y. Jiao, M. Jaroniec and S. Z. Qiao, *Angew. Chem. Int. Ed.*, 2012, **51**, 11496-11500.
34. B. Das, B. Choudhury, A. Gomathi, A. K. Manna, S. K. Pati and C. N. R. Rao, *ChemPhysChem*, 2011, **12**, 937-943.
35. Q. Bao, H. Zhang, J.-x. Yang, S. Wang, D. Y. Tang, R. Jose, S. Ramakrishna, C. T. Lim and K. P. Loh, *Adv. Funct. Mater.*, 2010, **20**, 782-791.
36. Y. He, N. Zhang, Q. Gong, H. Qiu, W. Wang, Y. Liu and J. Gao, *Carbohydr. Polym.*, 2012, **88**, 1100-1108.
37. N. Zhu, W. Liu, M. Xue, Z. Xie, D. Zhao, M. Zhang, J. Chen and T. Cao, *Electrochim. Acta*, 2010, **55**, 5813-5818.
38. W. S. Hummers and R. E. Offeman, *J. Am. Chem. Soc.*, 1958, **80**, 1339-1339.
39. M. Zhang, D. Lei, Z. Du, X. Yin, L. Chen, Q. Li, Y. Wang and T. Wang, *J. Mater. Chem.*, 2011, **21**, 1673-1676.
40. Z.-S. Wu, W. Ren, L. Gao, J. Zhao, Z. Chen, B. Liu, D. Tang, B. Yu, C. Jiang and H.-M. Cheng, *ACS Nano*, 2009, **3**, 411-417.
41. H. Wang, H. S. Casalongue, Y. Liang and H. Dai, *J. Am. Chem. Soc.*, 2010, **132**, 7472-7477.
42. S. Yi, J. Chen, H. Li, L. Liu, X. Xiao and X. Zhang, *Carbon*, 2010, **48**, 926-928.
43. C. V. Schenck, J. G. Dillard and J. W. Murray, *J. Colloid Interf. Sci.*, 1983, **95**, 398-409.
44. R. Dedryvère, S. Laruelle, S. Grugeon, P. Poizot, D. Gonbeau and J. M. Tarascon, *Chem. Mater.*, 2004, **16**, 1056-1061.
45. Z.-S. Wu, W. Ren, L. Wen, L. Gao, J. Zhao, Z. Chen, G. Zhou, F. Li and H.-M. Cheng, *ACS Nano*, 2010, **4**, 3187-3194.
46. D. Barreca, C. Massignan, S. Daolio, M. Fabrizio, C. Piccirillo, L. Armelao and E. Tondello, *Chem. Mater.*, 2001, **13**, 588-593.
47. L. Fu, Z. Liu, Y. Liu, B. Han, P. Hu, L. Cao and D. Zhu, *Adv. Mater.*, 2005, **17**, 217-221.
48. B. Varghese, C. H. Teo, Y. Zhu, M. V. Reddy, B. V. R. Chowdari, A. T. S. Wee, V. B. C. Tan, C. T. Lim and C. H. Sow, *Adv. Funct. Mater.*, 2007, **17**, 1932-1939.
49. Y. Wu, S. Fang and Y. Jiang, *Solid State Ionics*, 1999, **120**, 117-123.
50. Y. P. Wu, C. Y. Jiang, C. R. Wan, S. B. Fang and Y. Y. Jiang, *J. Appl. Poly. Sci.*, 2000, **77**, 1735-1741.

51. B. Zhang, Y. Yu, Z.-L. Xu, S. Abouali, M. Akbari, Y.-B. He, F. Kang and J.-K. Kim, *Adv. Energy Mater.*, 2013, DOI: 10.1002/aenm.201301448.
52. J.-H. Zhou, Z.-J. Sui, J. Zhu, P. Li, D. Chen, Y.-C. Dai and W.-K. Yuan, *Carbon*, 2007, **45**, 785-796.
53. B. Guo, X. Wang, P. F. Fulvio, M. Chi, S. M. Mahurin, X.-G. Sun and S. Dai, *Adv. Mater.*, 2011, **23**, 4661-4666.
54. C. F. Zhang, X. Peng, Z. P. Guo, C. B. Cai, Z. X. Chen, D. Wexler, S. Li and H. K. Liu, *Carbon*, 2012, **50**, 1897-1903.
55. C.-H. Lu and S.-W. Lin, *J. Power Sources*, 2001, **97–98**, 458-460.
56. X.-L. Huang, R.-Z. Wang, D. Xu, Z.-L. Wang, H.-G. Wang, J.-J. Xu, Z. Wu, Q.-C. Liu, Y. Zhang and X.-B. Zhang, *Adv. Funct. Mater.*, 2013, **23**, 4345-4353.
57. W. Yao, J. Chen and H. Cheng, *J. Solid State Electrochem.*, 2011, **15**, 183-188.
58. S. Xiong, J. S. Chen, X. W. Lou and H. C. Zeng, *Adv. Funct. Mater.*, 2012, **22**, 861-871.
59. J. Zhu, Y. K. Sharma, Z. Zeng, X. Zhang, M. Srinivasan, S. Mhaisalkar, H. Zhang, H. H. Hng and Q. Yan, *J. Phys. Chem. C*, 2011, **115**, 8400-8406.
60. C. Peng, B. Chen, Y. Qin, S. Yang, C. Li, Y. Zuo, S. Liu and J. Yang, *ACS Nano*, 2012, **6**, 1074-1081.
61. G. Wang, J. Liu, S. Tang, H. Li and D. Cao, *J. Solid State Electrochem.*, 2011, **15**, 2587-2592.
62. H. Zhang, H. Tao, Y. Jiang, Z. Jiao, M. Wu and B. Zhao, *J. Power Sources*, 2010, **195**, 2950-2955.
63. H.-X. Zhang, C. Feng, Y.-C. Zhai, K.-L. Jiang, Q.-Q. Li and S.-S. Fan, *Adv. Mater.*, 2009, **21**, 2299-2304.

